Inorg. Chem. **2003**, *42*, 5560–5571

Difference in Spin Crossover Pathways among Saddle-Shaped Six-Coordinated Iron(III) Porphyrin Complexes

Takahisa Ikeue,[†] Yoshiki Ohgo,[†] Owendi Ongayi,[‡] M. Graça H. Vicente,[‡] and Mikio Nakamura*[,†,§]

Department of Chemistry, School of Medicine, Toho University, Tokyo 143-8540, Japan, Division of Biomolecular Science, Graduate School of Science, Toho University, Funabashi 274-8510, Japan, and Department of Chemistry, Louisiana State University, Baton Rouge, Louisiana 70803-1804

Received March 13, 2003

The electronic states of a series of saddle-shaped porphyrin complexes $[Fe(OMTPP)L_2]^+$ and $[Fe(TBTXP)L_2]^+$ have been examined in solution by ^1H NMR, ^{13}C NMR, and EPR spectroscopy and by magnetic measurements. While $[Fe(OMTPP)(DMAP)_2]^+$ and $[Fe(TBTXP)(DMAP)_2]^+$ maintain the low-spin ($S = {}^1/_2$) state, $[Fe(OMTPP)(THF)_2]^+$ and $[Fe(TBTXP)(THF)_2]^+$ exhibit an essentially pure intermediate-spin ($S = {}^3/_2$) state over a wide range of temperatures. In contrast, the Py and 4-CNPy complexes of OMTPP and TBTXP exhibit a spin transition from $S = {}^3/_2$ to $S = {}^1/_2$ as the temperature was decreased from 300 to 200 K. Thus, the magnetic behavior of these complexes is similar to that of $[Fe(OETPP)Py_2]^+$ reported in our previous paper (Ikeue, T.; Ohgo, Y.; Yamaguchi, T.; Takahashi, M.; Takeda, M.; Nakamura, M. *Angew. Chem., Int. Ed.* **2001**, *40*, 2617–2620) in the context that all these complexes exhibit a novel spin crossover phenomenon in solution. Close examination of the NMR and EPR data of $[Fe(OMTPP)L_2]^+$ and $[Fe(TBTXP)L_2]^+$ (L = Py, 4-CNPy) revealed, however, that these complexes adopt the less common $(d_{xz}, d_{yz})^4(d_{xy})^1$ electron configuration at low temperature in contrast to $[Fe(OETPP)Py_2]^+$ which shows the common $(d_{xy})^2(d_{xz}, d_{yz})^3$ electron configuration. These observations have been attributed to the flexible nature of the OMTPP and TBTXP cores as compared with that of OETPP; the relatively flexible OMTPP and TBTXP cores can ruffle the porphyrin ring and adopt the $(d_{xz}, d_{yz})^4(d_{xy})^1$ electron configuration at low temperature. Therefore, this study reveals that the rigidity of porphyrin cores is an important factor in determining the spin crossover pathways.

Introduction

Several factors control the spin states of iron(III) porphyrin complexes.[1−3] Among these, the number and nature of axial ligands are the most important factors. Strong axial ligands such as cyanide, imidazole, and pyridine lead to the formation of low-spin ($S = {}^1/_2$) six-coordinate complexes. In contrast, anionic ligands such as Cl^- and F^- lead to the formation of five-coordinate high-spin ($S = {}^5/_2$) complexes. Maltempo[4] discussed a quantum mechanically spin admixed $S = {}^3/_2, {}^5/_2$ state and suggested that the $S = {}^3/_2$ state is an important contributor to the spin state of cytochromes *c*′, which are recognized as histidine ligated five-coordinate iron(III) complexes.[4−6] In fact, we have recently reported that the mono(imidazole) complexes of iron(III) porphyrins exhibit the $S = {}^3/_2, {}^5/_2$ admixed intermediate-spin state in a series of $[Fe(TMP)(RIm)]^+$ complexes, where RIm indicates alkyl substituted imidazoles and benzimidazoles.[7−9] In general, the $S = {}^3/_2$ character increases in five-coordinate complexes as the ligand field of anionic axial ligands weakens. Thus, Reed and co-workers ranked the relative field strengths of weak

* To whom correspondence should be addressed. E-mail: mnakamu@med.toho-u.ac.jp.
† School of Medicine, Toho Universirty.
‡ Louisiana State University.
§ Division of Biomolecular Science, Graduate School of Science, Toho University.

(1) Scheidt, W. R.; Reed, C. A. *Chem. Rev.* **1981**, *81*, 543−555.
(2) Scheidt, W. R.; Gouterman, M. In *Iron Porphyrin, Part I*; Lever, A. B. P., Gray, H. B., Eds.; Addison-Wesley: Reading, MA, 1983; pp 89−139.
(3) Scheidt, W. R. In *The Porphyrin Handbook*; Kadish, K. M., Smith, K. M., Guilard, R., Eds.; Academic Press: San Diego, CA, 2000; Vol. 3, Chapter 16, pp 49−112.
(4) Maltempo, M. M. J. *Chem. Phys.* **1974**, *61*, 2540−2547.
(5) Fujii, S.; Yoshimura, T.; Kamada, H.; Yamaguchi, K.; Suzuki, S.; Shidara, S.; Takakuwa, S. *Biochim. Biophys. Acta* **1995**, *1251*, 161−169.
(6) Déméné, H.; Tsan, P.; Gans, P.; Marion, D. *J. Phys. Chem. B* **2000**, *104*, 2559−2569.

10.1021/ic0300969 CCC: $25.00
Published on Web 08/15/2003

Scheme 1 Saddle and Ruffle Conformations for Nonplanar Distortion in the Porphyrin Core[a]

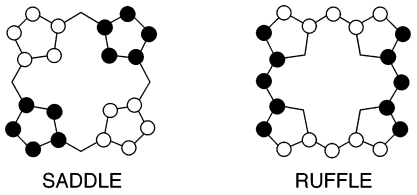

[a] Filled circles (●) correspond to atoms above the least squares plane (calculated for the 24 atoms of the porphyrin core), and open circles (○) represent atoms below the plane. Atoms not represented by circles are in the plane.

anionic ligands (X) in Fe(TPP)X on the basis of the spectroscopic and magnetic properties and called the hierarchy a magnetochemical series.[10,11] Recent studies have shown that the deformation of the porphyrin ring is also an important factor in determining the spin state;[12−14] a quite pure intermediate-spin state was observed in highly nonplanar six-coordinate complexes with weak axial ligands such as the saddled $[Fe(OETPP)(THF)_2]^+$ and the ruffled $[Fe(T^iPrP)(THF)_2]^+$ complexes.[12] The saddled and ruffled conformations are shown in Scheme 1. These results were attributed to the short Fe−N_p (N_p: nitrogen atoms of porphyrin) bond lengths caused by the nonplanarity of the porphyrin ring,[12−17] and the weak coordination ability of the axial ligands.[10,11] The pronounced S_4 saddled structure of the OETPP ring stabilizes the $S = {}^3/_2$ state even in the presence of nitrogen bases. Therefore, $[Fe(OETPP)(4\text{-}CNPy_2)]^+$ shows a quite pure intermediate-spin state over a wide range of temperatures in CD_2Cl_2 solution.[18] In sharp contrast, the ruffled porphyrin complex $[Fe(T^iPrP)(4\text{-}CNPy)_2]^+$ shows a typical low-spin character with $(d_{xz}, d_{yz})^4(d_{xy})^1$ electron configuration over a wide range of temperatures.[19] Obviously, the deformation mode of the porphyrin ring significantly influences the electron configuration of low-spin iron(III) and the spin state; we and others have shown that the ruffled deformation stabilizes the $(d_{xz}, d_{yz})^4(d_{xy})^1$ state,[19−29] while the saddled deformation stabilizes the $(d_{xy})^2(d_{xz}, d_{yz})^3$ state.[29] In this paper, we report on the spin states of other saddle-shaped porphyrin complexes, $[Fe(OMTPP)L_2]^+$ and $[Fe(TBTXP)L_2]^+$, in which the axial ligands are substituted pyridines and THF (Scheme 2). We also report that the magnetic behavior of $[Fe(OMTPP)L_2]^+$ and $[Fe(TBTXP)L_2]^+$ is significantly different from that of $[Fe(OETPP)L_2]^+$ despite the structural similarity of these complexes.

Scheme 2

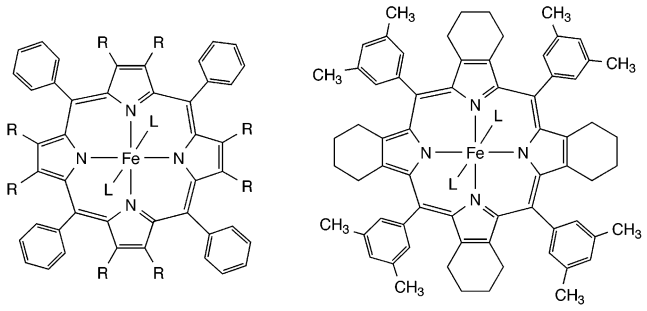

Experimental Section

General Procedure. ^1H and ^{13}C NMR spectra were recorded on a JEOL LA300 spectrometer operating at 300.4 MHz for ^1H. Chemical shifts were referenced to the residual peak of dichloromethane (δ = 5.32 ppm for ^1H and 53.8 ppm for ^{13}C). EPR spectra were measured at 4.2 K with a Bruker E500 spectrometer operating at X-band and equipped with an Oxford helium cryostat. The samples for the EPR measurement were prepared by the addition of ca. 10 mol equiv of ligands into the CH_2Cl_2 solutions of $[Fe(OMTPP)(THF)_2]ClO_4$. The concentrations of EPR samples were 5−8 mM. The observed EPR spectra had enough quality for the determination of the *g* values from the spectra. Solution magnetic moments of a series of $[Fe(OMTPP)L_2]ClO_4$ were determined by the Evans method in 5−7 mM CD_2Cl_2 solution.[30,31] Alumina (Merck, Brockmann Grade III) was used for column

(7) Abbreviations: ORTPP (R = M or E), dianion of 2,3,7,8,12,13,17,18-octaalkyl-5,10,15,20-tetraphenylporphyrin where R is methyl (M) or ethyl (E); TMP, TPP, and T^iPrP, dianions of 5,10,15,20-tetramesitylporphyrin, 5,10,15,20-tetraphenylporphyrin, and 5,10,15,20-tetraisopropylporphyrin; TBTXP and TBTPP, dianions of 2:3,7:8, 12:13,17:18-tetrabutano-5,10,15,20-tetra(3,5-dimethylphenyl)porphyrin and 2:3,7:8,12:13,17:18-tetrabutano-5,10,15,20-tetraphenylporphyrin; DMAP, 4-(*N*,*N*-dimethylamino)pyridine; Py, pyridine; 3-CNPy, 3-cyanopyridine; 4-CNPy, 4-cyanopyridine; HIm, imidazole; ^{t}BuNC, *tert*-butylisocyanide.
(8) Ikezaki, A.; Nakamura, M. *Chem. Lett.* **2000**, 994−995.
(9) Ikezaki, A.; Nakamura, M. *Inorg. Chem.* **2002**, *41*, 6225−6236.
(10) Reed, C. A.; Guiset, F. *J. Am. Chem. Soc.* **1996**, *118*, 3281−3282.
(11) Evans, D. R.; Reed, C. A. *J. Am. Chem. Soc.* **2000**, *122*, 4660−4667.
(12) Ikeue, T.; Saitoh, T.; Yamaguchi, T.; Ohgo, Y.; Nakamura, M.; Takahashi, M.; Takeda, M. *Chem. Commun.* **2000**, 1989−1990.
(13) Simonato, J.-P.; Pecaut, J.; Pape, L. L.; Oddou, J.-L.; Jeandey, C.; Shang, M.; Scheidt, W. R.; Wojacynski, J.; Wolowiec, S.; Latos-Grazynski, L.; Marchon, J.-C. *Inorg. Chem.* **2000**, *39*, 3978−3987.
(14) Weiss, R.; Gold, A.; Trautwein, A. X.; Terner, J. In *The Porphyrin Handbook*; Kadish, K. M., Smith, K. M., Guilard, R., Eds.; Academic Press: Burlington, MA, 2000; Vol. 3, pp 65−96.
(15) Ohgo, Y.; Saitoh, T.; Nakamura, M. *Acta Crystallogr.* **2001**, *C57*, 233−234.
(16) Ohgo, Y.; Saitoh, T.; Nakamura, M. *Acta Crystallogr.* **1999**, *C55*, 1284−1286.
(17) Nakamura, M.; Ikeue, T.; Ohgo, Y.; Takahashi, M.; Takeda, M. *Chem. Commun.* **2002**, 1198−1199.
(18) Ikeue, T.; Ohgo, Y.; Yamaguchi, T.; Takahashi, M.; Takeda, M.; Nakamura, M. *Angew Chem., Int. Ed.* **2001**, *40*, 2617−2620.
(19) Ikeue, T.; Ohgo, Y.; Saitoh, T.; Nakamura, M.; Fujii, H.; Yokoyama, M. *J. Am. Chem. Soc.* **2000**, *122*, 4068−4076.
(20) Walker, F. A. In *The Porphyrin Handbook*; Kadish, K. M., Smith, K. M., Guilard, R., Eds.; Academic Press: San Diego, CA, 2000; Vol. 5, Chapter 36, pp 81−183.
(21) Nakamura, M.; Ikeue, T.; Fujii, H.; Yoshimura, T. *J. Am. Chem. Soc.* **1997**, *119*, 6284−6291.
(22) Nakamura, M.; Ikeue, T.; Fujii, H.; Yoshimura, T.; Tajima, K. *Inorg. Chem.* **1998**, *37*, 2405−2414.
(23) Ikezaki, A.; Ikeue, T.; Nakamura, M. *Inorg. Chim. Acta* **2002**, *335*, 91−99.
(24) Wojaczynski, J.; Latos-Grazynski, L.; Glowiak, T. *Inorg. Chem.* **1997**, *36*, 6299−6306.
(25) Wolowiec, S.; Latos-Grazynski, L.; Mazzanti, M.; Marchon, J.-C. *Inorg. Chem.* **1997**, *36*, 5761−5771.
(26) Wolowiec, S.; Latos-Grazynski, L.; Toronto, D.; Marchon, J.-C. *Inorg. Chem.* **1998**, *37*, 724−732.
(27) Pilard, M.-A.; Guillemot, M.; Toupet, L.; Jordanov, J.; Simonneaux, G. *Inorg. Chem.* **1997**, *36*, 6307−6314.
(28) Simonneaux, G.; Schünemann, V.; Morice, C.; Carel, L.; Toupet, L.; Winkler, H.; Trautwein, A. X.; Walker, F. A. *J. Am. Chem. Soc.* **2000**, *122*, 4366.
(29) Ikeue, T.; Ohgo, Y.; Saitoh, T.; Yamaguchi, T.; Nakamura, M. *Inorg. Chem.* **2001**, *40*, 3423−3434.
(30) Evans, D. F. *J. Chem. Soc.* **1959**, 2003.
(31) Bertini, I.; Luchinat, C. In *NMR of Paramagnetic Molecules in Biological Systems*; Lever, A. B. P., Gray, H. B., Eds.; The Benjamin/Cummings: Menlo Park, CA, 1983; pp 130−133.

chromatography. Analytical thin-layer chromatography was performed using basic alumina or 60 F254 silica gel (precoated sheets, 0.2 mm thick). The syntheses were monitored by TLC and spectrophotometry. The electronic absorption spectra were measured in dichloromethane solution using a Perkin-Elmer Lambda 35 UV−vis spectrophotometer. Mass spectra were obtained at the LSU Mass Spectrometry Facility. 3,5-Dimethylbenzaldehyde, BF_3·OEt_2, dichlorodicyanobenzoquinone (DDQ), 1-nitrocyclohexene, 1,8-diazabicyclo-[5.4.0]undec-7-ene (DBU), and ethyl isocyanoacetate were purchased (Aldrich) and used without further purification. All solvents were dried and purified according to literature procedures.[32]

Synthesis. 2:3,7:8,12:13,17:18-Tetrabutano-5,10,15,20-tetra(3,5-dimethylphenyl)porphyrin, H_2(TBTXP) was prepared by the following method: Freshly distilled dry dichloromethane was added to a round-bottom flask fitted with a reflux condenser under argon. 3:4-Butanopyrrole (0.166 g, 1.37 mmol) and 3,5-dimethylbenzaldehyde (0.18 mL, 1.37 mmol) were added, and the solution was stirred at room temperature under a slow steady stream of argon for 15 min. The flask was shielded from light, and BF_3·OEt_2 (0.02 mL, 0.137 mmol) was added.[33] This mixture was then stirred for 1 h at room temperature. DDQ (1.50 g, 6.60 mmol) was added to the reaction flask, and the final solution turned dark pink instantly. This mixture was refluxed under argon for 1 h to give a dark green solution. The solvent was reduced to dryness under vacuum, and the resulting residue was purified by column chromatography using dichloromethane for elution. Recrystallization from methanol gave purple crystals of the title porphyrin (0.18 g, 56% yield). ^{1}H NMR ($CDCl_3$, drop of d-TFA) 8.00 (s, 8H, o-ArH), 7.51 (s, 4H, p-ArH), 2.70 (s, 24H, *m*-CH_3), 2.37, 2.02, 1.72, and 1.29 (broad s, 8H each, CH_2), −0.50 (s, 4H, 4NH). UV−Vis of dication (CH_2Cl_2, λ_{max} nm) 461 (ϵ 283 800), 671 (24 700). MS (MALDI) *m*/*e* 944.28 (M^+).

H_2(OMTPP), *meso*-^{13}C enriched H_2(OMTPP), Fe(OMTPP)Cl, and Fe(TBTXP)Cl were prepared according to the literature.[29,34−36] [Fe(OMTPP)(THF)$_2$]ClO_4 and [Fe(TBTXP)(THF)$_2$]ClO_4 were prepared by addition of a THF solution of $AgClO_4$ to THF solutions of Fe(OMTPP)Cl and Fe(TBTXP)Cl.[29,37] A series of bis-ligated complexes, [Fe(OMTPP)L_2]ClO_4 and [Fe(TBTXP)L_2]ClO_4, were prepared by addition of 10−15 equiv of the ligand such as DMAP, Py, 3-CNPy, 4-CNPy, HIm, and ^{t}BuNC to a CH_2Cl_2 or a CD_2Cl_2 solution of [Fe(OMTPP)(THF)$_2$]ClO_4.[29]

Results and Discussion

Formation of the Bis-Ligated Complexes. (i) OMTPP Complexes. Pyridine usually behaves as a weaker ligand than imidazole and cyanide. Therefore, it is important to confirm that the complexes examined in this study actually have bis-coordination of the ligand even at room temperature. Figure 1 shows the ^{1}H NMR spectra of the sample obtained after addition of various amounts of 4-CNPy to a CD_2Cl_2 solution of [Fe(OMTPP)(THF)$_2$]$^+$ at 298 K. When 3.1 equiv of 4-CNPy was added, two broad signals assigned to 4-CNPy were observed downfield at 41.5 and 26.1 ppm. Figure 2a shows the change in chemical shift of these signals upon addition of 4-CNPy. The gradual upfield shift of the ligand protons suggests that the coordinated ligand is rapidly exchanging with the free ligand on the ^{1}H NMR time scale at room temperature.

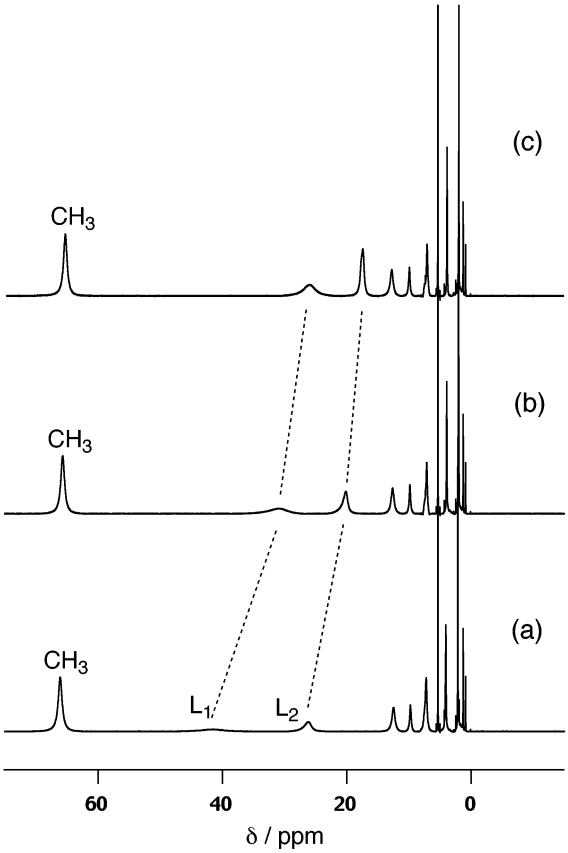

Figure 1. ^{1}H NMR spectra obtained upon addition of (a) 3.1 equiv, (b) 5.6 equiv, and (c) 9.0 equiv of 4-CNPy to a CD_2Cl_2 solution of [Fe(OMTPP)(THF)$_2$]$^+$ at 298 K.

The porphyrin signals, on the other hand, exhibited only small changes. For example, the methyl signal appeared at 66.1, 65.7, and 64.7 ppm, and the *p*-phenyl signal appeared at 9.7, 9.8, and 9.9 ppm when 3.1, 5.6, and 9.0 equiv of 4-CNPy were added, respectively. Thus, the chemical shifts of the porphyrin protons are almost independent of the amount of ligand added, which indicates that [Fe(OMTPP)-(THF)$_2$]$^+$ is mostly converted into [Fe(OMTPP)(4-CNPy)$_2$]$^+$ at least by the addition of 9.0 equiv of 4-CNPy. It should be noted, however, that the chemical shifts of the methyl and *p*-phenyl protons obtained by addition of excess ligand were not significantly different from those of starting [Fe(OMTPP)(THF)$_2$]$^+$; the chemical shifts of the methyl and *p*-phenyl protons in [Fe(OMTPP)(THF)$_2$]$^+$ are 62.0 and 7.6 ppm, respectively. Thus, this conclusion should be taken with reservation.

More conclusive evidence of the formation of [Fe-(OMTPP)(4-CNPy)$_2$]$^+$ was obtained from the observed changes in chemical shift for the THF protons. In [Fe-(OMTPP)(THF)$_2$]$^+$, the THF protons were observed at 11.6 and 7.6 ppm. Upon addition of 4-CNPy, these signals shifted upfield and approached those of free THF as is shown in

(32) Perrin, D. D.; Armarego, W. L. F. In *Purification of Laboratory Chemicals*, 3rd ed.; Pergamon Press: Oxford, 1988.
(33) Medforth, C. J.; Berber, M. D.; Smith, K. M.; Shelnutt, J. A. *Tetrahedron Lett.* **1990**, *31*, 3719−3722.
(34) Barkigia, K. M.; Berber, M. D.; Fajer, J.; Medforth, C. J.; Renner, M. W.; Smith, K. M. *J. Am. Chem. Soc.* **1990**, *112*, 8851−8857.
(35) Sparks, L. D.; Medforth, C. J.; Park, M.-S.; Chamberlain, J. R.; Ondrias, M. R.; Senge, M. O.; Smith, K. M.; Shelnutt, J. A. *J. Am. Chem. Soc.* **1993**, *115*, 581−592.
(36) Cheng, R.-J.; Chen, P.-Y.; Gau, P.-R.; Chen, C.-C.; Peng, S.-M. *J. Am. Chem. Soc.* **1997**, *119*, 2563−2569.
(37) Ogoshi, H.; Sugimoto, H.; Watanabe, E.; Yoshida, Z.; Maeda, Y.; Sakai, H. *Bull. Chem. Soc. Jpn.* **1981**, *54*, 3414−3419.

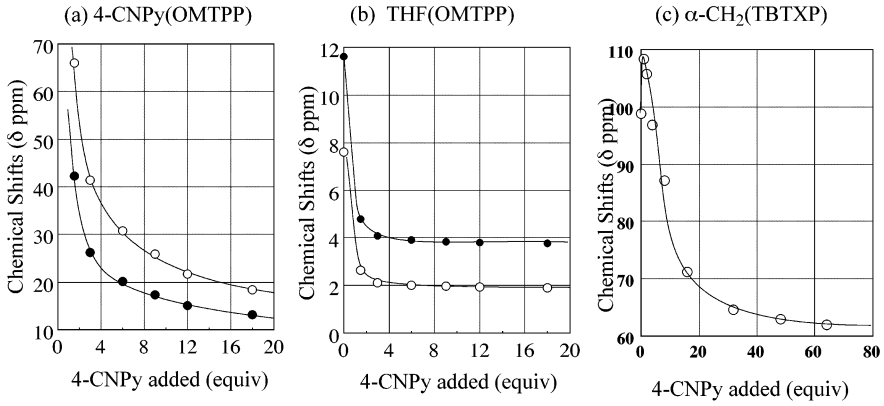

Figure 2. Change in chemical shifts of (a) 4-CNPy and (b) THF protons in $[Fe(OMTPP)(THF)_2]^+$ at 298 K and (c) α-methylene protons in $[Fe(TBTXP)(THF)_2]^+$ at 273 K upon addition of 4-CNPy.

Figure 2b. When 9.0 equiv of 4-CNPy was added, two sharp THF signals appeared at 1.93 and 3.80 ppm. The integral intensities of these signals were similar to those of the *ortho* and *meta* phenyl protons. These results strongly indicate that the coordinated THF ligands are completely replaced by 4-CNPy at least when 9.0 equiv of the ligand is added.

(ii) TBTXP Complexes. The formation of bis-ligated complexes in the TBTXP system was also confirmed by titration experiments. As already mentioned, the methyl signal of $[Fe(OMTPP)]ClO_4$ showed only a small change by addition of 4-CNPy. In contrast, the α-methylene signal of $[Fe(TBTXP)]ClO_4$ exhibited a significant shift. Figure 2c shows the change in chemical shifts of the α-methylene protons upon addition of 4-CNPy at 0 °C. When 1.0 equiv of 4-CNPy was added, the signal moved downfield from 98.9 to 108.4 ppm. Further addition of the ligand up to 64 equiv caused a gradual upfield shift of the signal until it reached a constant value of 62.1 ppm. Therefore, it is reasonable to assume that the signals at 108.4 and 62.1 ppm are the α-methylene protons of the mono- and bis-adducts, respectively. The chemical shifts of $[Fe(TBTXP)(4\text{-}CNPy)_2]^+$ at various temperatures were determined by using the sample containing 64 equiv of the ligand. Addition of a large excess of 4-CNPy is not necessary for the formation of the bis-adduct at lower temperature; the chemical shift of the α-methylene signal of the sample containing 8 equiv of 4-CNPy is nearly the same as that containing 64 equiv of the ligand below 230 K. The bis-coordination of the other porphyrin complexes was similarly confirmed.

Spin States of $[Fe(OMTPP)L_2]^+$ in Solution. (i) ^{1}H NMR Spectra. Porphyrin ring protons give characteristic ^{1}H NMR signals which depend on the electronic state of the paramagnetic metal ions. Thus, ^{1}H NMR spectroscopy has been frequently used to determine the spin state of iron(III) porphyrin complexes.[38−41] We have recently reported the ^{1}H NMR spectra of a series of bis-ligated complexes such as $[Fe(OMTPP)L_2]^{\pm}$ (L = HIm, CN^-, ^{t}BuNC) and $[Fe(OETPP)L_2]^{\pm}$ (L = HIm, CN^-, ^{t}BuNC, DMAP, Py, 4-CNPy, THF).[12,18,29] The ^{1}H NMR chemical shifts of $[Fe(OETPP)(1\text{-}MeIm)_2]^+$ have also been recently reported.[42] Characteristic features of the ^{1}H NMR chemical shifts based on these studies are summarized as follows: (i) High-spin ($S = {}^5/_2$) complexes such as Fe(OMTPP)Cl and Fe(OETPP)Cl show the methyl and methylene signals fairly downfield, δ 20−50 ppm, at room temperature.[35,36,42−45] (ii) Low-spin ($S = {}^1/_2$) complexes with the common $(d_{xy})^2(d_{xz}, d_{yz})^3$ electron configuration such as $[Fe(OMTPP)(HIm)_2]^+$ and $[Fe(OETPP)(HIm)_2]^+$ also exhibit downfield methyl and methylene signals, 4−20 ppm at room temperature.[29] (iii) Low-spin ($S = {}^1/_2$) complexes with the less common $(d_{xz}, d_{yz})^4(d_{xy})^1$ electron configuration such as $[Fe(OMTPP)(^tBuNC)_2]^+$ and $[Fe(OETPP)(^tBuNC)_2]^+$ show the *meta*-phenyl protons at 11−13 ppm, which are similar to those of the high-spin complexes.[29] However, the methyl and methylene signals appear upfield, 0−10 ppm, in these complexes in contrast to those of the high-spin complexes. (iv) Intermediate-spin ($S = {}^3/_2$) complexes such as $[Fe(OETPP)(THF)_2]^+$ and $[Fe(OETPP)(4\text{-}CNPy)_2]^+$ exhibit downfield shifted methylene signals, 12−50 ppm.[12,19] The presence of downfield shifted *ortho* and *para* signals is another characteristic feature of intermediate-spin complexes since in the other spin states, $S = {}^1/_2$ and $S = {}^5/_2$, the complexes do not show downfield shifted *ortho* and *para* protons; the *ortho* and *para* signals of $[Fe(OETPP)(4\text{-}CNPy)_2]^+$ appear at 13.9 and 12.0 ppm, respectively, at room temperature.[18]

The spin states of a series of complexes $[Fe(OMTPP)L_2]^+$ (L = DMAP, Py, and 4-CNPy) were examined on the

(38) Walker, F. A.; Simonis, U. In *NMR of Paramagnetic Molecules*; Berliner, L. J., Reuben, J., Eds.; Plenum Press: New York, 1993; Vol. 12, pp 133−274.
(39) Goff, H. M. In *Iron Porphyrin, Part I*; Lever, A. B. P., Gray, H. B., Eds.; Addison-Wesley: Reading, MA, 1983; pp 237−281.
(40) Bertini, I.; Luchinat, C. In *NMR of Paramagnetic Substances*; Lever, A. B. P., Ed.; Elsevier: Amsterdam, 1996; pp 29−75.
(41) Bertini, I.; Luchinat, C. In *NMR of Paramagnetic Molecules in Biological Systems*; Lever, A. B. P., Gray, H. B., Eds.; The Benjamin/Cummings: Menlo Park, CA, 1983; pp 165−229.
(42) Ogura, H.; Yatsunyk, L.; Medforth, C. J.; Smith, K. M.; Barkigia, K. M.; Renner, M. W.; Melamed, D.; Walker, F. A. *J. Am. Chem. Soc.* **2001**, *123*, 6564−6578.
(43) Nakamura, M.; Yamaguchi, T.; Ohgo, Y. *Inorg. Chem.* **1999**, *38*, 3126−3131.
(44) [Fe(OETPP)Cl] was reported to be an $S = {}^5/_2$ spin state with approximately 40% $S = {}^3/_2$ spin admixture.[36] A later report has shown that the $S = {}^3/_2$ contribution is much smaller, 4−10%.[45]
(45) Schünemann, V.; Gerdan, M.; Trautwein, A. X.; Haoudi, N.; Mandon, D.; Fischer, J.; Weiss, R.; Tabard, A.; Guilard, R. *Angew Chem., Int. Ed.* **1999**, *38*, 3181−3183.

Table 1. ^{1}H NMR Chemical Shifts of $[Fe(ORTPP)L_2]^+$(R = Me, Et) and $[Fe(TBTXP)L_2]^+$ Taken in CD_2Cl_2 Solution at 273, 193, and 173 K

	Py-CH						ortho-H			meta-H[c]			para-H			
L	273		193		173		273	193	173	273	193	173	273	193	173	ref
								OMTPP								
HIm	19.4		23.0		25.1		4.4	1.8	0.8	5.8	4.4	3.9	6.4	5.4	5.0	29
DMAP[a]	18.8		21.8		23.0		4.5	2.1	1.1	6.1	5.0	4.6	6.4	5.5	5.1	this work
Py	39.6		22.6		23.1		9.1	4.1	3.5	7.2	8.0	8.0	8.4	6.3	6.1	this work
4-CNPy	65.4		36.9		23.5		13.8	7.5	5.3	6.6	9.6	11.5	10.5	7.9	6.8	this work
THF[a]	67.0		91.3		101.2		13.0	17.6	19.6	7.0	5.9	5.8	10.2	12.1	13.8	this work
^{t}BuNC[a]	0.5		−3.9		−5.1		2.5	−0.2	−1.3	13.4	16.3	17.5	4.9	3.6	3.2	29
								OETPP								
HIm[a,b]	4.1	10.8	2.7	12.8	2.2	13.6	4.3	1.5	0.4	5.5	3.9	3.5	6.5	5.6	5.3	29
DMAP[a,b]	4.4	12.0	2.6	13.1	1.9	13.4	4.6	1.2	−0.4	5.6	4.2	3.7	6.6	5.5	4.9	18
Py[a]	10.4	32.0	6.5	23.7	4.4	22.0	12.2	4.8	2.6	5.6	4.8	5.7	10.0	6.8	5.9	18
4-CNPy	17.2	45.8	21.1	64.3	22.2	70.9	14.1	14.6	14.9	5.0	3.6	3.0	12.5	14.6	15.3	18
THF[a]	15.2	45.7	25.7	59.8	22.9	64.1	12.7	11.1	10.0	6.1	4.4	3.4	11.1	13.6	14.8	12
^{t}BuNC		7.8	5.6	18.1	6.2	22.5	5.5	6.7	7.4	11.2	11.4	11.0	6.3	6.8	6.2	29
								TBTXP								
HIm[a]	28.1		32.4		34.9		4.7	2.7	2.2	1.8	1.2	1.0	6.2	5.4	5.1	this work
DMAP[a]	25.2		31.5		34.0		4.4	2.4	1.6	1.8	1.2	1.1	6.2	5.4	5.0	this work
Py[a]	27.7		21.7		22.0		5.7	4.1	4.0	2.4	2.2	2.2	6.9	6.6	6.7	this work
4-CNPy	62.1		14.2		12.4		*c*	3.7	4.3	3.3	2.4	2.4	8.2	6.6	6.5	this work
3-CNPy	94.1		48.7		27.7		12.5	6.8	4.5	4.0	2.9	2.6	9.4	7.5	6.9	this work
THF[a]	98.7		146.8		165.8		*c*	12.2	12.8	3.7	4.0	4.2	8.7	9.1	9.3	this work
^{t}BuNC	−1.5		−4.6		−1.7	−9.6	*d*	*d*	*d*	2.0	1.7	1.6	*d*	*d*	*d*	this work

[a] Data at 173 K were obtained by the extrapolation from the high temperature data. [b] Data at 298 K were obtained by the extrapolation from the low temperature data. [c] Chemical shifts of *m*-CH_3 in the case of $[Fe(TBTXP)L_2]^+$. [d] Signals are too broad.

basis of the spectroscopic characteristics already described. The chemical shifts in Table 1 and the Curie plots for the methyl and *meta*-proton signals in Figure 3A clearly indicate that $[Fe(OMTPP)(DMAP)_2]^+$ is in the low-spin state at least below 273 K because of the similarity of the chemical shifts and their temperature dependence to those of $[Fe(OMTPP)(HIm)_2]Cl$; the latter has been fully characterized as the low-spin complex with $(d_{xy})^2(d_{xz}, d_{yz})^3$ electron configuration.[29] In contrast, the methyl signal of $[Fe(OMTPP)Py_2]^+$ exhibited a curious temperature dependence as shown in Figure 3Aa. While it appeared fairly downfield, 53.1 ppm at room temperature, it moved upfield and approached the methyl signal of $[Fe(OMTPP)(HIm)_2]^+$ at 173 K. The methyl signal of $[Fe(OMTPP)(4\text{-}CNPy)_2]^+$ also appeared fairly downfield, 61.9 ppm at 313 K. This signal moved downfield as the temperature was lowered from 313 to 273 K and then shifted upfield as the temperature was further lowered from 273 to 173 K. At 173 K, the lowest temperature examined in this NMR study, the methyl signal of $[Fe(OMTPP)(4\text{-}CNPy)_2]^+$ appeared very close to that of the low-spin $[Fe(OMTPP)(HIm)_2]^+$ complex. These results suggest that the spin transition from the $S = {}^3/_2$ to the $S = {}^1/_2$ took place both in $[Fe(OMTPP)Py_2]^+$ and $[Fe(OMTPP)(4\text{-}CNPy)_2]^+$ in the temperature range 313−173 K as observed in the case of $[Fe(OETPP)(Py)_2]^+$ reported in our previous paper.[18] The presence of the downfield shifted *ortho* and *para* protons at room temperature and their upfield shift at lower temperature also support the spin transition. The unexpected result was obtained, however, from the Curie plots for the *meta* signals shown in Figure 3Ab. As the temperature was lowered, the Curie line of the *meta* signal of $[Fe(OMTPP)(4\text{-}CNPy)_2]^+$ moved away from that of $[Fe(OMTPP)(HIm)_2]^+$, and approached that of $[Fe(OMTPP)(^t BuNC)_2]^+$. Similar temperature dependence was observed in $[Fe(OMTPP)(Py)_2]^+$ although the deviation from the Curie line for $[Fe(OMTPP)(HIm)_2]^+$ was less pronounced than that for $[Fe(OMTPP)(4\text{-}CNPy)_2]^+$. Since $[Fe(OMTPP)(^t BuNC)_2]^+$ has been well characterized as the low-spin complex with a quite pure $(d_{xz}, d_{yz})^4(d_{xy})^1$ electron configuration on the basis of ^{1}H NMR, ^{13}C NMR, and EPR spectroscopy,[29] the most reasonable explanation is that the spin transition takes place from the $S = {}^3/_2$ to the $S = {}^1/_2$ in both $[Fe(OMTPP)(4\text{-}CNPy)_2]^+$ and $[Fe(OMTPP)Py_2]^+$,[18,45−47] and that the $S = {}^1/_2$ complexes formed at low temperature adopt the $(d_{xz}, d_{yz})^4(d_{xy})^1$ electron configuration. This is in sharp contrast to the case of the corresponding OETPP complex, $[Fe(OETPP)Py_2]^+$, where the spin transition occurs from the $S = {}^3/_2$ to the $S = {}^1/_2$ with the $(d_{xy})^2(d_{xz}, d_{yz})^3$ electron configuration.[18] The reasons for the difference in spin crossover pathways between the OMTPP and OETPP complexes will be discussed later. It is worthwhile to compare the electronic ground state of $[Fe(OMTPP)(4\text{-}CNPy)_2]^+$ with that of $[Fe(TMP)(4\text{-}CNPy)_2]^+$ reported by Walker et al.[48,49] Comparison of the ^{1}H NMR chemical shifts of these complexes clearly demonstrates that the $(d_{xz}, d_{yz})^4(d_{xy})^1$ contribution in $[Fe(TMP)(4\text{-}CNPy)_2]^+$ is much larger than that in $[Fe(OMTPP)(4\text{-}CNPy)_2]^+$; the chemical shifts of the *meta* signals of $[Fe(TMP)(4\text{-}CNPy)_2]^+$ and $[Fe(OMTPP)(4\text{-}CNPy)_2]^+$ are 14.6 and 9.6 ppm, respectively, at 193 K. In other words, the energy difference between the d_{xy} and $d_\pi(d_{xz}, d_{yz})$ orbitals is much larger in

(46) Hodges, K. D.; Wollmann, R. G.; Kessel, S. L.; Hendrickson, D. N.; VanDerveer, D. G.; Barefield, E. K. *J. Am. Chem. Soc.* **1979**, *101*, 906−917.
(47) Koch, W. O.; Schünemann, V.; Gerdan, M.; Trautwein, A. X.; Krüer, H.-J. *Chem. Eur. J.* **1998**, *4*, 686−691.
(48) Safo, M. K.; Gupta, G. P.; Watson, C. T.; Simonis, U.; Walker, F. A.; Scheidt, W. R. *J. Am. Chem. Soc.* **1992**, *114*, 7066−7075.
(49) Safo, M. K.; Walker, F. A.; Raitsimring, A. M.; Walters, W. P.; Dolata, D. P.; Debrunner, P. G.; Scheidt, W. R. *J. Am. Chem. Soc.* **1994**, *116*, 7760−7770.

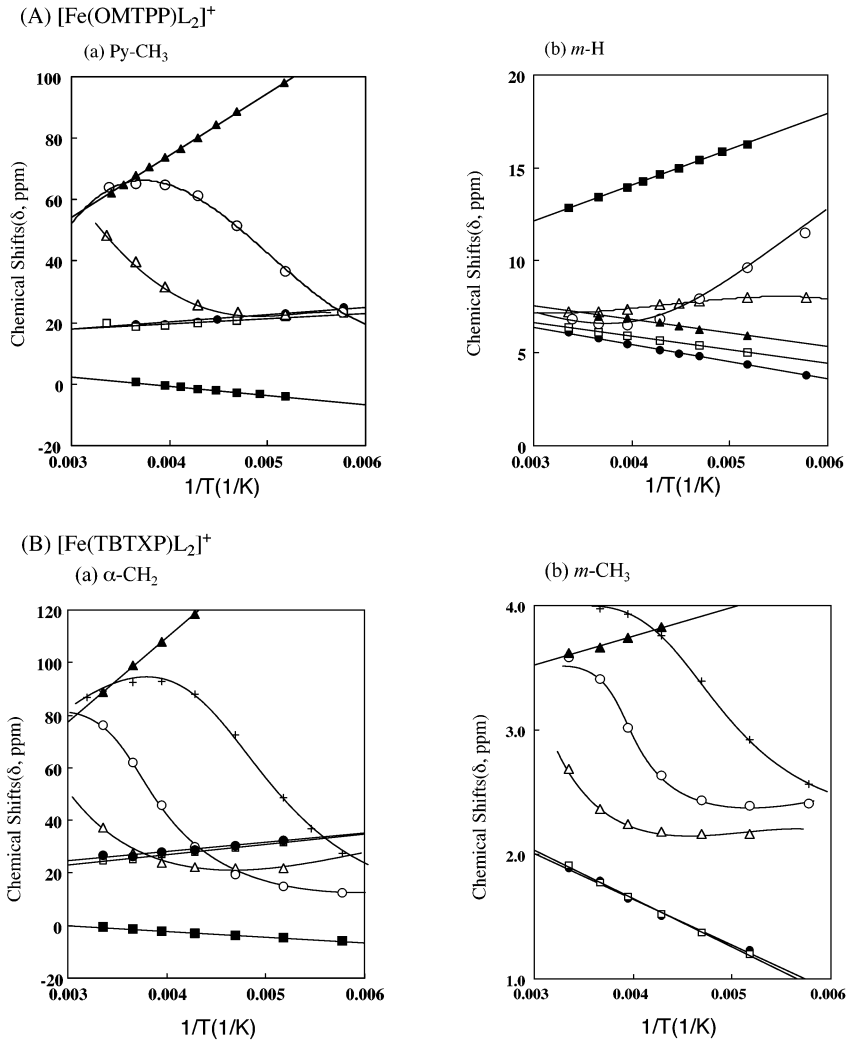

Figure 3. Curie plots for some signals of (A) $[Fe(OMTPP)L_2]^+$ and (B) $[Fe(TBTXP)L_2]^+$ in CD_2Cl_2 solution. (A) (a) Py-CH_3 and (b) *m*-H; (B) (a) α-CH_2 and (b) *m*-CH_3 signals: □, DMAP; △, Py; ○, 4-CNPy; +, 3-CNPy; ▲, THF; ●, HIm; ■, ^{t}BuNC.

$[Fe(TMP)(4\text{-}CNPy)_2]^+$ than in $[Fe(OMTPP)(4\text{-}CNPy)_2]^+$. Similarly, the *meta* signal of $[Fe(TMP)Py_2]^+$ appears at 9.5 ppm, which is 1.5 ppm more downfield than that in $[Fe(OMTPP)Py_2]^+$; note that the downfield shift of the *meta* signal is caused by the increase in the $(d_{xz}, d_{yz})^4(d_{xy})^1$ contribution.[23,29,48] These results are consistent with our recent finding that saddle-shaped complexes resist changing their electron configuration from the common $(d_{xy})^2(d_{xz}, d_{yz})^3$ to the less common $(d_{xz}, d_{yz})^4(d_{xy})^1$ even if the axial ligands have weak σ-donating and strong π-accepting characters.[29]

In the case of $[Fe(OMTPP)(THF)_2]^+$, the methyl signal appeared fairly downfield, 62.1 ppm at room temperature, and moved further downfield in proportion to $1/T$. Thus, the complex is expected to be in the intermediate-spin state as in the case of $[Fe(OETPP)(THF)_2]^+$.[12] The presence of the downfield shifted *ortho* and *para* signals, 17.6 and 12.1 ppm at 193 K, respectively, is another piece of evidence showing that the complex is in the intermediate-spin state.[12,18]

(ii) Solution Magnetic Moments. Temperature dependence of the effective magnetic moments of $[Fe(OMTPP)L_2]^+$ (L = DMAP, Py, 4-CNPy, THF) has been determined by the Evans method in CD_2Cl_2 solution and is given in Figure 4. $[Fe(OMTPP)(DMAP)_2]^+$ exists almost exclusively as the low-spin complex in the temperature range 213−280 K. $[Fe(OMTPP)Py_2]^+$ also exists as the low-spin complex

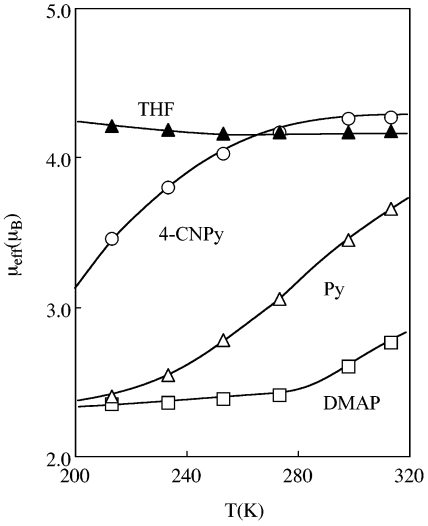

Figure 4. Temperature dependence of the effective magnetic moments of a series of $[Fe(OMTPP)L_2]^+$ species determined in CD_2Cl_2 solution by the Evans method.

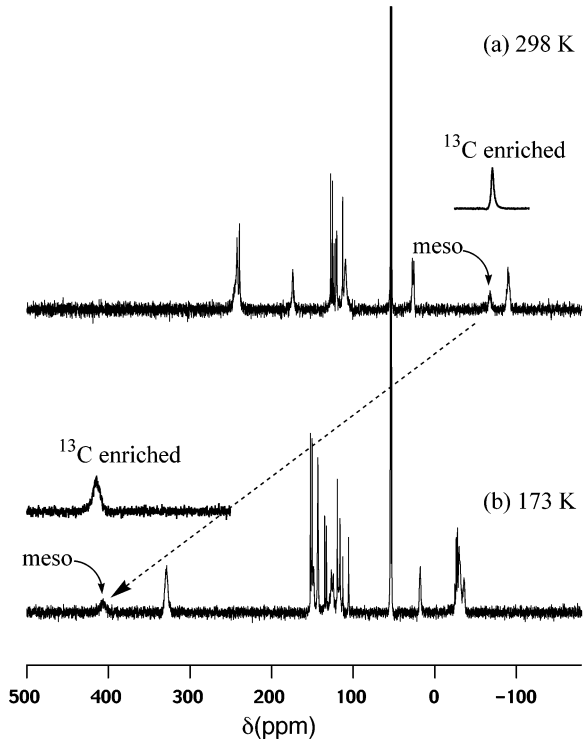

Figure 5. ^{13}C NMR spectra of $[Fe(OMTPP)(4\text{-}CNPy)_2]^+$ taken in CD_2Cl_2 solution at (a) 298 K and (b) 173 K.

at 213 K, although the intermediate-spin complex increases steeply as the temperature is raised. In the case of $[Fe(OMTPP)(4\text{-}CNPy)_2]^+$, both the low-spin and intermediate-spin complexes exist comparably even at 213 K. The intermediate-spin complex increased with the temperature and became the sole entity at 280 K. The effective magnetic moments of $[Fe(OMTPP)(THF)_2]^+$ are almost constant, 4.1−4.2 μ_B, in the temperature range 213−280 K, indicating that the complex is in the intermediate-spin state. Thus, the results on the effective magnetic moments are consistent with those obtained by ^{1}H NMR spectroscopy.

(iii) ^{13}C NMR Spectra. Figure 5 shows the ^{13}C NMR spectra of $[Fe(OMTPP)(4\text{-}CNPy)_2]^+$ taken at 298 and 173 K. The signals were assigned on the basis of the acquisition of the proton-coupled ^{13}C NMR spectra. The *meso*-carbon signals were assigned using *meso*-^{13}C enriched complexes. The α-pyrrole and *ipso*-phenyl carbons of $[Fe(OMTPP)(DMAP)_2]^+$ and $[Fe(OMTPP)Py_2]^+$ were conveniently assigned on the basis of their coupling with the adjacent *meso*-carbons in the ^{13}C NMR spectra of the *meso*-^{13}C enriched complexes.[29] In the inset of Figure 5 are given the ^{13}C NMR spectra of the *meso*-^{13}C enriched complexes taken at 298 and 173 K. Table 2 lists the ^{13}C NMR chemical shifts of the *meso*, Py-α, and Py-*β* carbons in $[Fe(OMTPP)L_2]^+$ taken at 298, 193, and 173 K along with those of the corresponding carbons in $[Fe(OETPP)L_2]^+$.[18,29] Figure 6 shows the Curie plots for the *meso*-carbon signals of a series of $[Fe(OMTPP)L_2]^+$ complexes. As suggested from the ^{1}H NMR chemical shifts, $[Fe(OMTPP)(DMAP)_2]^+$ is in the low-spin state since the chemical shift of the *meso* signal and its temperature dependence are quite similar to those of $[Fe(OMTPP)(HIm)_2]^+$ over the temperature range examined.[29] In contrast,

Table 2. ^{13}C NMR Chemical Shifts of $[Fe(ORTPP)L_2]^+$ (R = Me, Et) Taken in CD_2Cl_2 Solution at 298, 193, and 173 K

	meso			Py-α		Py-*β*		
L	298	193	173	298	193	298	193	ref
				OMTPP				
HIm	29.9	−36.6	−57.5	128.4	74.8	173.0	161.3	29
DMAP	48.0	3.4	−13.9	109.8	49.9	163.7	147.2	this work
Py	−8.8	163.3	180.1.	204.6	42.1	214.4	157.8	this work
4-CNPy	−67.9	224.3	422.5	242.5	109.0	242.0	188.1	this work
THF	−0.5	−104.7	−138.8[a]	*b*	*b*	*b*	*b*	this work
^{t}BuNC	701.4	1153[a]		−206.5	−484.0[a]	112.8	77.2[a]	29
				OETPP				
HIm	7.3	−65.1	−87.1	163.0	130.5	167.0	148.5	29
DMAP	2.5	−52.7	−81.1	167.9	122.1	175.9	159.4	18
Py	−186.2	−88.0	−73.6	384.1	224.0	243.8	211.2	18
4-CNPy	−235.6	−499.5	−510.6	469.6	664.0	265.6	328.1	18
THF	−87.0	−291.4[a]		*b*	*b*	*b*	*b*	this work
^{t}BuNC	419.3	340.8	232[a]	−3.7	74.3	144.2	137.0	29

[a] Data obtained by the extrapolation from high temperature. [b] Signals are too broad to detect.

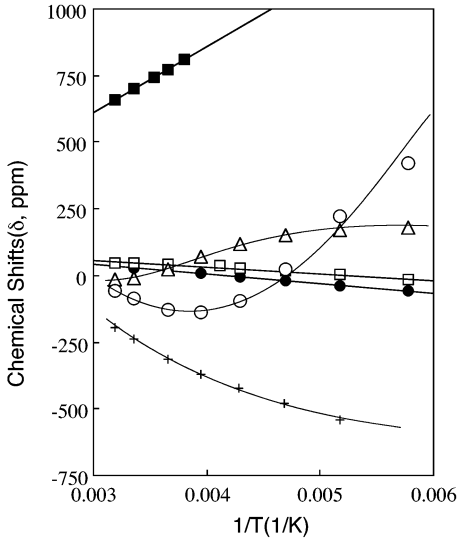

Figure 6. Curie plots for the *meso*-^{13}C signals of $[Fe(OMTPP)L_2]^+$ and $[Fe(OETPP)(4\text{-}CNPy)_2]^+$ taken in CD_2Cl_2 solution. The following symbols are used for the $[Fe(OMTPP)L_2]^+$ complexes: □, DMAP; △, Py; ○, 4-CNPy; ●, HIm; ■, ^{t}BuNC. The symbol + indicates the *meso*-carbon signal of $[Fe(OETPP)(4\text{-}CNPy)_2]^+$.

the *meso* signal of $[Fe(OMTPP)(4\text{-}CNPy)_2]^+$ showed a completely different temperature dependence. It appeared fairly upfield, −67.9 ppm at 298 K, and moved further upfield until the temperature was lowered to 253 K where it reached −138 ppm. The presence of a fairly upfield shifted *meso* signal is one of the most characteristic features of the intermediate-spin complexes which discriminates them from the complexes in different spin states such as $S = {}^1/_2$ and $S = {}^5/_2$; the *meso*-carbon signals are usually observed at δ = 0−100 ppm in the $(d_{xy})^2(d_{xz}, d_{yz})^3$-type low-spin complexes,[29,38−41] δ > 200 ppm in the $(d_{xz}, d_{yz})^4(d_{xy})^1$-type low-spin complexes,[19,22,23,29] and ca. 500 ppm in the high-spin complexes.[38−41] Some low-spin complexes with quite pure $(d_{xz}, d_{yz})^4(d_{xy})^1$ electron configuration such as $[Fe(TPP)(^tBuNC)_2]^+$ exhibit the *meso* signals fairly downfield, at around 800 ppm.[29] Thus, the ^{13}C NMR data indicate that the major part of $[Fe(OMTPP)(4\text{-}CNPy)_2]^+$ is in the $S = {}^3/_2$ state at 298−253 K. As the temperature was further lowered below 253 K, the *meso* signal of $[Fe(OMTPP)(4\text{-}CNPy)_2]^+$

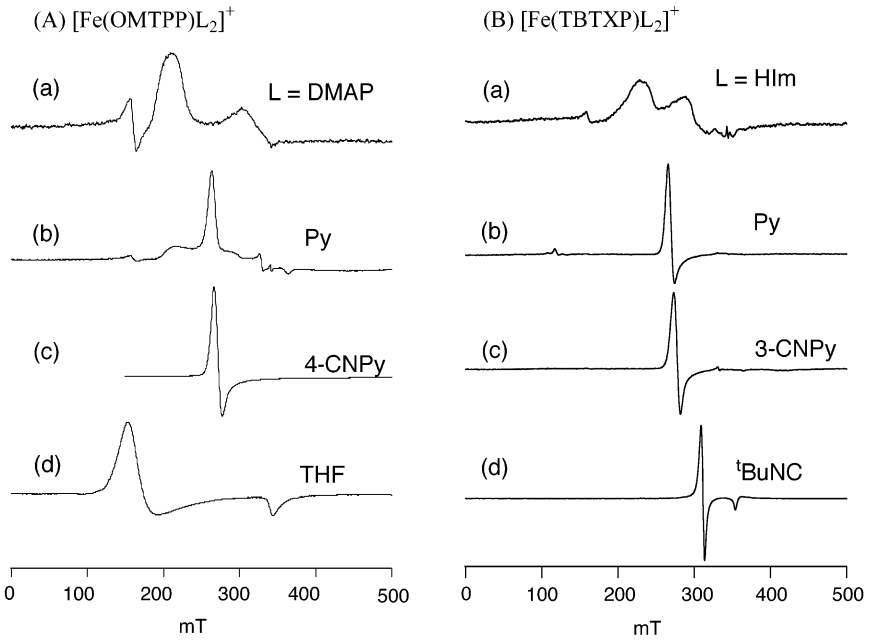

Figure 7. EPR spectra of (A) $[Fe(OMTPP)L_2]^+$ and (B) $[Fe(TBTXP)L_2]^+$ taken in frozen CH_2Cl_2 solutions at 4.2 K.

steeply moved downfield and reached 423 ppm at 173 K. The large downfield shift of the *meso* signal strongly indicates that the low-spin complex with $(d_{xz}, d_{yz})^4(d_{xy})^1$ electron configuration exists as a major component.[19,22,23,29,50] Thus, the spin transition takes place from the $S = {}^3/_2$ to the $S = {}^1/_2$ with $(d_{xz}, d_{yz})^4(d_{xy})^1$ electron configuration as the temperature is lowered.

Similar spin transition has been observed in $[Fe(OMTPP)Py_2]^+$ although the population of the $S = {}^3/_2$ state is comparable to that of the $S = {}^1/_2$ even at 298 K as it is revealed from the chemical shift of the *meso* signal, −8.8 ppm. As already mentioned, the *meso* signals of $[Fe(OMTPP)(HIm)_2]^+$ and $[Fe(OMTPP)(4\text{-}CNPy)_2]ClO_4$ appeared at 29.9 and −67.9 ppm, respectively; the former complex is considered to be in the pure low-spin state with $(d_{xy})^2(d_{xz}, d_{yz})^3$ electron configuration,[29] while the latter is in an essentially pure intermediate-spin state at 298 K based on the effective magnetic moment shown in Figure 4. As the temperature was lowered to 173 K, the *meso* signal moved downfield from −8.8 to 180.1 ppm, suggesting that the complex is in the low-spin state with $(d_{xz}, d_{yz})^4(d_{xy})^1$ electron configuration. Thus, the temperature dependence of the magnetic behavior of $[Fe(OMTPP)Py_2]^+$ and $[Fe(OMTPP)(4\text{-}CNPy)_2]^+$ resembles that of $[Fe(OETPP)Py_2]^+$ in the sense that all these complexes exhibit a novel spin transition from the $S = {}^3/_2$ to the $S = {}^1/_2$; $[Fe(OETPP)(4\text{-}CNPy)_2]^+$ exhibits the spin transition only in the solid state below 180 K.[18] It should be emphasized again that the electron configurations of the low-spin complexes formed at low temperature are different; $[Fe(OMTPP)Py_2]^+$ and $[Fe(OMTPP)(4\text{-}CNPy)_2]^+$ adopt the $(d_{xz}, d_{yz})^4(d_{xy})^1$ electron configuration while $[Fe(OETPP)Py_2]^+$ forms the $(d_{xy})^2(d_{xz}, d_{yz})^3$ electron configuration.

We have already mentioned on the basis of the ^1H NMR and solution magnetic moments that both $[Fe(OMTPP)(THF)_2]^+$ and $[Fe(OMTPP)(4\text{-}CNPy)_2]^+$ exhibit an essentially pure intermediate-spin state at room temperature. The chemical shifts of the *meso*-carbons are, however, quite different; while $[Fe(OMTPP)(THF)_2]^+$ showed the *meso* signal at −0.5 ppm at room temperature, $[Fe(OMTPP)(4\text{-}CNPy)_2]^+$ exhibited it at −67.9 ppm. Even the *meso* signal of $[Fe(OMTPP)Py_2]^+$, which has much smaller $S = {}^3/_2$ character than $[Fe(OMTPP)(THF)_2]^+$, appeared more upfield, −8.8 ppm. A similar tendency has been observed in the OETPP series; although both $[Fe(OETPP)(THF)_2]^+$ and $[Fe(OETPP)(4\text{-}CNPy)_2]^+$ are pure intermediate-spin complexes, the chemical shifts of their *meso* signals are very different, −87 and −236 ppm, respectively, at 298 K.[18] The reason for this difference in *meso*-carbon shifts will be discussed in detail later in this paper. Nevertheless, the ^{13}C NMR results are totally consistent with those obtained by ^1H NMR and magnetic measurements.

(iv) EPR Spectra. Figure 7A shows the EPR spectra of $[Fe(OMTPP)L_2]^+$ taken at 4.2 K in frozen CH_2Cl_2 solution. Table 3 lists the EPR g values for $[Fe(OMTPP)\text{-}L_2]^+$. The g values for saddled $[Fe(OETPP)L_2]^+$ and ruffled $[Fe(T^iPrP)\text{-}L_2]^+$ are also listed for comparison.[12,18,19,29,51] EPR spectroscopy has been frequently used to determine the electronic state of iron(III) porphyrins. While high-spin complexes give signals at $g = 6$ and 2, intermediate-spin complexes exhibit signals at $g = 4$ and 2.[52] In the case of six-coordinate low-spin complexes, there are three types of EPR spectra.[20,53,54]

(50) Nakamura, M.; Ikeue, T.; Ikezaki, A.; Ohgo, Y.; Fujii, H. *Inorg. Chem.* **1999**, *38*, 3857−3862.
(51) Ikeue, T.; Yamaguchi, T.; Ohgo, Y.; Nakamura, M. *Chem. Lett.* **2000**, 342−343.
(52) Palmer, G. In *Iron Porphyrin, Part II*; Lever, A. B. P., Gray, H. B., Eds.; Addison-Wesley: Reading, MA, 1983; pp 43−88.
(53) Walker, F. A.; Reis, D.; Balke, V. L. *J. Am. Chem. Soc.* **1984**, *106*, 6888−6898.
(54) Walker, F. A.; Huynh, B. H.; Scheidt, W. R.; Osvath, S. R. *J. Am. Chem. Soc.* **1986**, *108*, 5288−5297.

Table 3. EPR g Values of Nonplanar Six-Coordinate Iron(III) Porphyrin Complexes Taken at 4.2 K in Frozen CH_2Cl_2 Solution

porphyrin	L	g_1	g_2	g_3	ref
OMTPP	HIm	2.84	2.31	1.58	29
	DMAP	3.21	2.06		this work
	Py	2.53	2.53	1.85	this work
	4-CNPy	2.52	2.52	1.82	this work
	THF	4.09	4.09	1.97	this work
	^{t}BuNC	2.20	2.17	1.95	29
OETPP	HIm	2.72	2.37	1.64	29
	DMAP	3.24			51
	Py[a]	3.39	2.08		18
	4-CNPy[a]	4.28	3.80	2.08	18
	THF	4.01	4.01	2.00	12
	^{t}BuNC	2.29	2.25	1.92	29
TBTXP	HIm	2.99	2.29		this work
	DMAP	3.12			this work
	Py	2.54	2.54		this work
	3-CNPy	2.50	2.50		this work
	4-CNPy	2.49	2.49		this work
	THF	4.05	4.05	1.99	this work
	^{t}BuNC	2.21	2.21	1.94	this work
T^{i}PrP	HIm	2.55	2.55		29
	DMAP	2.54	2.54		19
	Py	2.52	2.52	1.60	19
	4-CNPy	2.41	2.41	1.79	19
	THF	3.99	3.99	1.97	12
	^{t}BuNC	2.16	2.16	1.96	29

[a] Taken for the solid samples.

The first is the rhombic spectrum consisting of three signals, and it is observed in complexes carrying two planar axial ligands aligned in a parallel fashion above and below the porphyrin ring. The second is the so-called large g_{max} type spectrum in which two planar ligands are oriented perpendicularly. Complexes with linear ligands such as cyanide also show large g_{max} type.[20,21,50,55] While these two types of spectra are observed in complexes with $(d_{xy})^2(d_{xz}, d_{yz})^3$ electron configuration, the third known as the axial type is observed in complexes with $(d_{xz}, d_{yz})^4(d_{xy})^1$ electron configuration; the latter complexes generally have axial ligands with low lying π^* orbitals and/or a strongly ruffled porphyrin ring.[20,22,29]

The EPR spectrum of $[Fe(OMTPP)(DMAP)_2]^+$ shown in Figure 7Aa is classified as the large g_{max} type as in the case of $[Fe(OETPP)(DMAP)_2]^+$.[18,42,51] Thus, $[Fe(OMTPP)(DMAP)_2]^+$ is a low-spin complex with $(d_{xy})^2(d_{xz}, d_{yz})^3$ electron configuration at 4.2 K. In contrast, the EPR spectrum of $[Fe(OMTPP)(4\text{-}CNPy)_2]^+$ shown in Figure 7Ac is classified as the axial type, which indicates that the complex adopts the $(d_{xz}, d_{yz})^4(d_{xy})^1$ electron configuration. The lack of signals corresponding to the intermediate-spin complex and/or the low-spin complex with $(d_{xy})^2(d_{xz}, d_{yz})^3$ electron configuration should be attributed to the temperature effect. This means that the populations of these species decrease at lower temperature and become negligibly small at 4.2 K, the temperature at which the EPR spectra are measured. Although the EPR spectrum of $[Fe(OMTPP)Py_2]^+$ shown in Figure 7Ab consists of at least two components, the large g_{max} and axial types, the major part is the axial type as in the case of $[Fe(OMTPP)(4\text{-}CNPy)_2]^+$.[55−57] Thus, $[Fe(OMTPP)Py_2]^+$ exists mainly as the low-spin complex with $(d_{xz}, d_{yz})^4(d_{xy})^1$ electron configuration at 4.2 K although the complex with $(d_{xy})^2(d_{xz}, d_{yz})^3$ electron configuration also exists as a minor component. The EPR spectrum of $[Fe(OMTPP)(THF)_2]^+$ shown in Figure 7Ad exhibits two signals at $g =$ 4.09 and 1.97, indicating that the complex is in a quite pure intermediate-spin state as in the case of the corresponding OETPP complex $[Fe(OETPP)(THF)_2]^+$.[12] Therefore, the EPR results are consistent with those obtained by other methods such as ^{1}H and ^{13}C NMR spectroscopy and the magnetic data.

Spin States of $[Fe(TBTXP)L_2]^+$ in Solution. (i) ^{1}H NMR Spectra. The chemical shifts of a series of $[Fe(TBTXP)L_2]^+$ (L = DMAP, Py, 4-CNPy, 3-CNPy, THF, HIm, and ^{t}BuNC) species are listed in Table 1. The Curie plots of the α-methylene and *meta*-methyl signals are given in Figure 3B. These results suggest that the spin state of $[Fe(TBTXP)L_2]^+$ resembles that of $[Fe(OMTPP)L_2]^+$ when the axial ligand is the same. For example, $[Fe(TBTXP)(THF)_2]^+$ adopts the $S = {}^3/_2$ state as is revealed by the downfield shifted α-methylene signal, 166 ppm at 173 K, along with its linearity in the Curie plots. A fairly large downfield shift of the α-methylene signal as compared with that of $[Fe(OMTPP)(THF)_2]^+$, 101 ppm at 173 K, should be attributed to the difference in dihedral angle between the H−C_α−C(β-pyrrole) plane and the pyrrole ring; one of the α-methylene protons in the cyclohexene ring of the TBTXP complex is supposed to be parallel to the p_z orbital at the β-pyrrole carbon,[59,60] and therefore suffers a large contact shift.[38−40] Similarly, $[Fe(TBTXP)(DMAP)_2]^+$ and $[Fe(TBTXP)(HIm)_2]^+$ adopt the $S = {}^1/_2$ spin state over a wide temperature range as observed in $[Fe(OMTPP)(DMAP)_2]^+$ and $[Fe(OMTPP)(HIm)_2]^+$. In contrast to the complexes already mentioned, the Curie plots for the α-CH_2 and *m*-CH_3 protons of $[Fe(TBTXP)(3\text{-}CNPy)_2]^+$, $[Fe(TBTXP)(4\text{-}CNPy)_2]^+$, and $[Fe(TBTXP)Py_2]^+$ exhibited curvatures, which suggests a spin crossover phenomenon between the $S = {}^3/_2$ and the $S = {}^1/_2$. Since the Curie lines of the α-methylene signals in these complexes moved away from those of $[Fe(TBTXP)(HIm)_2]^+$ and $[Fe(TBTXP)(DMAP)_2]^+$ at lower temperature, and approached the Curie line of $[Fe(TBTXP)(^t\text{BuNC})_2]^+$ as shown in Figure 3B, the electron configuration of the low-spin complexes formed at 173 K should be represented as $(d_{xz}, d_{yz})^4(d_{xy})^1$. Therefore, the temperature dependence of the magnetic behavior in $[Fe(TBTXP)(4\text{-}CNPy)_2]^+$ and $[Fe(TBTXP)Py_2]^+$ is quite similar to that of the corresponding OMTPP complexes.

(ii) EPR Spectra. The EPR spectra of a series of $[Fe(TBTXP)L_2]^+$ complexes were taken in frozen CH_2Cl_2 solutions at 4.2 K and are shown in Figure 7B. The g values

(55) Inniss, D.; Soltis, S. M.; Strouse, C. E. *J. Am. Chem. Soc.* **1988**, *110*, 5644−5650.

(56) The low-spin complexes with the $(d_{xy})^2(d_{xz}, d_{yz})^3$ and $(d_{xz}, d_{yz})^4(d_{xy})^1$ electron configurations should be considered as isomers and exist as the different entities at 4.2 K;[57] the former maintains the saddled structure while the latter has the saddled structure with ruffled contribution.[58]

(57) Ikezaki, A.; Nakamura, M. *Inorg. Chem.* **2002**, *41*, 2761−2768.
(58) Shelnutt, J. A.; Song, X.-Z.; Ma, J.-G.; Jia, S.-L.; Jentzen, W.; Medforth, C. *J. Chem. Soc. Rev.* **1998**, *27*, 31−41.
(59) Barkigia, K. M.; Renner, M. K.; Furenlid, L. R.; Medforth, C. J.; Smith, K. M.; Fajer, J. *J. Am. Chem. Soc.* **1993**, *115*, 3627−3635.
(60) Finikova, O. S.; Cheprakov, A. V.; Carroll, P. J.; Dalosto, S.; Vinogradov, S. A. *Inorg. Chem.* **2002**, *41*, 6944−6946.

Scheme 3. Schematic Representation of the Change in Energy Levels of the Iron d Orbitals at Ambient Temperature in Solution Expected When Planar TPP Is Replaced by Saddled ORTPP (R = Me, Et), or When the Axial Ligand in $[Fe(ORTPP)L_2]ClO_4$ Changes from DMAP to Py, to 4-CNPy, and Then to THF[a]

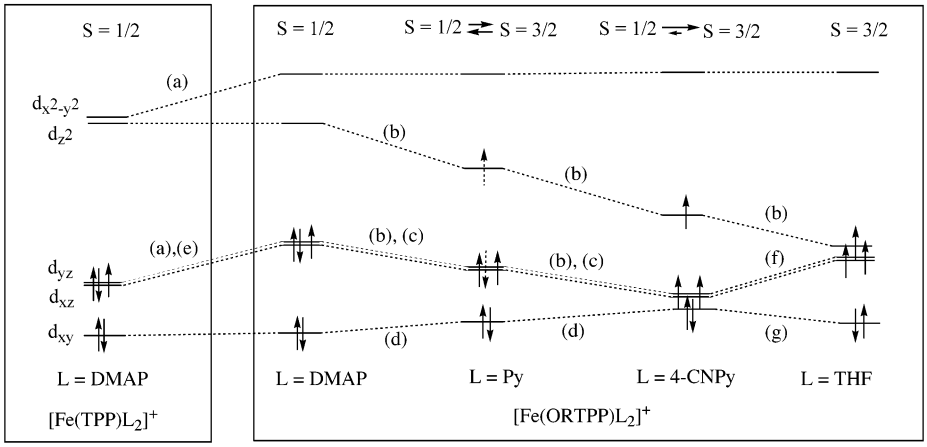

[a] Labels a−g indicate the stabilization or destabilization of the iron d orbitals caused by the ligand change: (a) destabilization due to short $Fe-N_p$ bond lengths caused by the saddled deformation; (b) stabilization due to the weak ligand field of axial ligand; (c) stabilization due to the iron d_π and ligand p_π^* interactions; (d) destabilization due to the iron d_{xy} and porphyrin a_{2u} interaction; (e) destabilization due to the increase in the interaction between iron d_π and porphyrin $3e_g$ orbitals; (f) destabilization due to the lack of the iron d_π and ligand p_π^* interactions; (g) stabilization due to the lack of the iron d_{xy} and porphyrin a_{2u} interaction.

are listed in Table 3. The results are similar to those in the corresponding $[Fe(OMTPP)L_2]^+$ complexes with the same axial ligand. Both the DMAP and HIm complexes show the low-spin state with $(d_{xy})^2(d_{xz}, d_{yz})^3$ electron configuration while the Py, 3-CNPy, and 4-CNPy complexes exhibit the low-spin state with $(d_{xz}, d_{yz})^4(d_{xy})^1$ electron configuration at 4.2 K. As expected, the ^{t}BuNC showed a typical axial spectrum with $g_\perp = 2.21$ and $g_{||} = 1.94$, suggesting that the complex is in a quite pure low-spin state with $(d_{xz}, d_{yz})^4(d_{xy})^1$ electron configuration. In the case of $[Fe(TBTXP)(THF)_2]^+$, two signals were observed at $g = 4.05$ and 1.99, indicating that the complex is in the intermediate-spin state as in the case of $[Fe(OMTPP)(THF)_2]^+$ and $[Fe(OETPP)(THF)_2]^+$ complexes.

Reasons for the Novel Magnetic Behavior in Saddled $[Fe(ORTPP)L_2]^+$ (R = Me, Et) and $[Fe(TBTXP)L_2]^+$. In the present paper as well as in our previous papers,[18,61] we have reported that saddle-shaped complexes $[Fe(OMTPP)L_2]^+$ (L = Py, 4-CNPy) and $[Fe(OETPP)L_2]^+$ (L = Py) commonly exhibit a spin crossover process between the $S = {}^3/_2$ and $S = {}^1/_2$ in solution. The magnetic behavior of these complexes can be interpreted in terms of the difference in energy levels of the five d orbitals. In the following discussion, we explain why these complexes exhibit a novel spin transition as the temperature is lowered. Scheme 3 is a qualitative illustration of how the energy levels of the d orbitals vary when going from planar $[Fe(TPP)(DMAP)_2]^+$ to saddled $[Fe(ORTPP)(DMAP)_2]^+$, $[Fe(ORTPP)Py_2]^+$, $[Fe(ORTPP)(4\text{-}CNPy)_2]^+$, and then $[Fe(ORTPP)(THF)_2]^+$. In the saddled complexes, the $d_{x^2-y^2}$ orbital is destabilized due to the short $Fe-N_p$ bond distances.[36,42,45,61−63] The short $Fe-N_p$ bond distances also destabilize the $d_\pi(d_{xz}, d_{yz})$ orbitals due to the stronger $d_\pi-3e_g$ interactions as compared with those in the planar complexes having longer $Fe-N_p$ bond distances.[29] The effective overlaps of the d_π and $3e_g$ orbitals expected for the saddled conformation could further strengthen these interactions.[29] In this situation, if the axial DMAP ligand is replaced by Py and then by 4-CNPy ligands, the energy level of the d_{z^2} orbital drops to a great extent due to the weak ligand field strength of 4-CNPy. Concomitantly, the energy levels of the d_π orbitals also drop due to the iron-$(d_\pi)-$ligand(p_{π^*}) interactions although the degree of decrease in the d_π orbitals is expected to be much smaller than that in the d_{z^2} orbital. As a result, the d_{z^2} and d_π orbitals in $[Fe(ORTPP)(4\text{-}CNPy)_2]^+$ are located quite close to each other in the energy diagram, which results in the formation of the intermediate-spin complex at room temperature. When the temperature is lowered, an iron−ligand bond contraction can occur.[61,64,65] This contraction could cause the increase in energy level of the d_{z^2} orbital and induce the spin transition from the $S = {}^3/_2$ to the $S = {}^1/_2$. It should be noted here that, while $[Fe(OETPP)Py_2]^+$ adopts the $(d_{xy})^2(d_{xz}, d_{yz})^3$ electron configuration, $[Fe(OMTPP)Py_2]^+$ and $[Fe(OMTPP)(4\text{-}CNPy)_2]^+$ have the $(d_{xz}, d_{yz})^4(d_{xy})^1$ electron configuration at low temperature.

The difference in the electron configurations between the OMTPP and OETPP systems at low temperature can be explained as follows. When DMAP is replaced by Py, the energy levels of the d_π orbitals are lowered due to the iron-$(d_\pi)-$ligand(p_π^*) interactions in both systems. These complexes are further stabilized by the $d_{xy}-a_{2u}$ interaction caused by the ruffling of the porphyrin core. In the previous paper, we mentioned that the OETPP core is more rigid than the OMTPP core on the basis of the difference in the rotation barriers of the coordinated 2-MeIm ligands between [Fe-

(61) Ohgo, Y.; Ikeue, T.; Nakamura, M. *Inorg. Chem.* **2002**, *41*, 1698−1700.
(62) Cheng, R.-J.; Chen, P.-Y. *Chem. Eur. J.* **1999**, *5*, 1708−1715.
(63) Barkigia, K. M.; Renner, M. W.; Fajer, J. *J. Porphyrins Phthalocyanines* **2001**, *5*, 415−418.
(64) Scheidt, W. R.; Geiger, D. K.; Haller, K. J. *J. Am. Chem. Soc.* **1982**, *104*, 495−499.
(65) Ellison, M. K.; Nasri, H.; Xia, Y.-M.; Marchon, J.-C.; Schulz, C. E.; Debrunner, P. G.; Scheidt, W. R. *Inorg. Chem.* **1997**, *36*, 4801−4811.

Scheme 4. Schematic Representation of the Change in Energy Levels of the Iron d Orbitals at Ambient Temperature Expected When Planar TPP Is Replaced by Ruffled T^{i}PrP, or When the Axial Ligand in [Fe(T^{i}PrP)L_2]ClO_4 Changes from DMAP to Py, to 4-CNPy, and Then to THF[a]

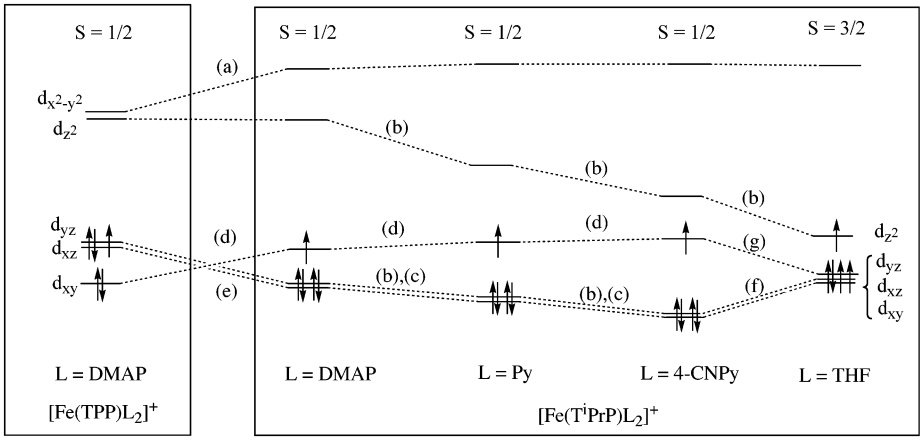

[a] Labels a−g indicate the stabilization or destabilization of the iron d orbitals expected for the ligand change: (a) destabilization due to short Fe−N_p bond lengths caused by the ruffled deformation; (b) stabilization due to the weak ligand field of axial ligand; (c) stabilization due to the iron d_π and ligand p_π* interactions; (d) destabilization due to the iron d_{xy} and porphyrin a_{2u} interaction; (e) stabilization due to the decrease in interactions between the iron d_π and porphyrin $3e_g$ orbitals; (f) destabilization due to the lack of the iron d_π and ligand p_π* interactions; (g) stabilization due to the lack of the iron d_{xy} and porphyrin a_{2u} interaction.

(OMTPP)(2-MeIm)$_2$]$^+$ and [Fe(OETPP)(2-MeIm)$_2$]$^+$; the *meso*-carbon signal of the latter complex splits into three signals below −60 °C due to the hindered rotation of the ligand while the corresponding signal in the former complex maintains its singlet even at −100 °C.[29] Another set of evidence supporting the rigidity of the OETPP core as compared to the OMTPP core comes from the difference in chemical shifts of the *meso*-^{13}C signals between [Fe(OMTPP)(^{t}BuNC)$_2$]$^+$ and [Fe(OETPP)(^{t}BuNC)$_2$]$^+$; the *meso*-^{13}C signals were observed at 701 and 419 ppm at 25 °C, respectively. A larger downfield shift of the *meso*-^{13}C signal in the OMTPP complex corresponds to the greater $(d_{xz}, d_{yz})^4(d_{xy})^1$ contribution, which in turn corresponds to the larger ruffling of the OMTPP core.[29] We can then explain why only the OMTPP complexes, [Fe(OMTPP)Py_2]$^+$ and [Fe(OMTPP)(4-CNPy)$_2$]$^+$, adopt the $(d_{xz}, d_{yz})^4(d_{xy})^1$ electron configuration; the OMTPP complexes can ruffle the porphyrin core with relatively small energy and change the electron configuration from $(d_{xy})^2(d_{xz}, d_{yz})^3$ to $(d_{xz}, d_{yz})^4(d_{xy})^1$.[66]

The flexibility of the TBTXP core as compared with that of the OETPP core can be understood from the results reported by Smith, Shelnutt, and co-workers; the inversion barrier of [Ni(TBTPP)], which is structurally similar to TBTXP, is much smaller than that of [Ni(OETPP)] as determined by the line shape analysis of the ^{1}H NMR signals.[33] In the present case, the temperature dependence of the diastereotopic α-methylene protons also showed a large difference in ^{1}H NMR line shape between [Fe(TBTXP)L_2]$^+$ and [Fe(OETPP)L_2]$^+$. For example, a broad α-methylene signal of [Fe(OETPP)(DMAP)$_2$]$^+$ at 25 °C splits into two signals below 0 °C. In contrast, the α-methylene signal of [Fe(TBTXP)(DMAP)$_2$]$^+$ maintained a broad singlet even at −80 °C. A similar difference in temperature dependence of the α-methylene signals was observed for the HIm, Py, and 4-CNPy complexes. Thus, the ring inversion of the TBTXP complexes takes place more rapidly than that of the OETPP complexes, which in turn indicates the flexible nature of the TBTXP core as compared to the OETPP core. The present study therefore reveals that the rigidity of the porphyrin ring plays a crucial role in determining the spin crossover pathways.

Reasons for the Formation of [Fe(ORTPP)(THF)$_2$]$^+$ (R = Me, Et) with an Essentially Pure Intermediate-Spin State. As shown in Scheme 3, the replacement of 4-CNPy with a much weaker THF ligand could induce several changes in the energy levels of the d orbitals: (i) stabilization of the d_{z^2} orbital, (ii) stabilization of the d_{xy} orbital, and (iii) destabilization of the d_π orbitals. The stabilization of the d_{z^2} orbital is attributed to the weak ligand field of THF as compared with 4-CNPy. The latter two effects, ii and iii, are caused by the lack of π-accepting capability of THF. Because the iron (d_π) and ligand (p_π*) interactions are fairly weak in [Fe(ORTPP)(THF)$_2$]$^+$, the energy levels of the d_π orbitals would be raised when going from [Fe(ORTPP)(4-CNPy)$_2$]$^+$ to [Fe(ORTPP)(THF)$_2$]$^+$. As a result, the d_π orbitals are located far above the d_{xy} orbital, which in turn weakens the iron (d_{xy}) and porphyrin (a_{2u}) interactions and hence stabilizes the iron (d_{xy}) orbital; note that the destabilization of the iron d_{xy} orbital is caused by the $d_{xy}-a_{2u}$ interaction in the low-spin complexes with $(d_{xz}, d_{yz})^4(d_{xy})^1$ electron configuration.[48,49] Therefore, the three d orbitals, d_{xz}, d_{yz}, and d_{z^2}, are located quite close to each other, resulting in the formation of an essentially pure intermediate-spin complex over a wide range of temperatures.

In the previous section, we mentioned that the upfield shift of the *meso*-carbon signal is the most characteristic feature of intermediate-spin complexes from the viewpoint of ^{13}C

(66) Our preliminary result on the X-ray crystallographic analysis of [Fe(OMTPP)Py_2]ClO_4 has revealed that the saddled deformation of this complex is much smaller than that of [Fe(OETPP)Py_2]ClO_4 previously reported;[61] the average deviation of the β-pyrrole carbon atoms from the least-squares porphyrin plane is 1.04 Å in the former while it is 1.22 Å in the latter. The result is another piece of evidence supporting the rigid nature of the OETPP core as compared to the OMTPP core. Ohgo, Y.; Ikeue, T.; Takahashi, M.; Takeda, M.; Nakamura, M. To be published.

NMR spectroscopy. Although both $[Fe(ORTPP)(THF)_2]^+$ and $[Fe(ORTPP)(4\text{-}CNPy)_2]^+$ are in the $S = {}^3/_2$ spin state at least at room temperature, the chemical shifts of the *meso*-carbon signals are quite different; they are -0.5 (R = Me) and -87.0 (R = Et) ppm for $[Fe(ORTPP)(THF)_2]^+$ and -67.9 (R = Me) and -235.6 (R = Et) ppm for $[Fe(ORTPP)(4\text{-}CNPy)_2]^+$. As previously mentioned, the d_π orbitals of $[Fe(ORTPP)(THF)_2]^+$ are located far above those of the corresponding $[Fe(ORTPP)(4\text{-}CNPy)_2]^+$ as shown in Scheme 3. Therefore, the iron(d_π)−porphyrin($3e_g$) interactions are more effective in $[Fe(ORTPP)(4\text{-}CNPy)_2]^+$ than in $[Fe(ORTPP)(THF)_2]^+$ due to the smaller energy gap in the former complexes. Since the $3e_g$ orbitals have large coefficients at the pyrrole carbon and nitrogen and zero spin density at the *meso*-carbon atoms,[38] the strong iron(d_π)−porphyrin($3e_g$) interactions in $[Fe(ORTPP)(4\text{-}CNPy)_2]^+$ induce larger spin densities on the pyrrole carbon atoms, which in turn causes a large downfield shift of the pyrrole carbon signal and an upfield shift of the adjacent *meso*-carbon signal.[19,23,29,67] As a result, the *meso* signals of the 4-CNPy complexes appear at greater magnetic field at room temperature than those of the corresponding THF complexes.

Difference in Magnetic Properties between Saddled $[Fe(ORTPP)L_2]^+$ (R = Me, Et) and Ruffled $[Fe(TRP)L_2]^+$. The energy levels of the d orbitals in ruffled complexes such as $[Fe(T^iPrP)L_2]^+$ are influenced differently by the porphyrin ring.[19] The ruffling of the planar porphyrin ring causes three major effects on the d orbitals of bis-ligated iron(III) porphyrins: (i) destabilization of the $d_{x^2-y^2}$ orbital due to the short Fe−N_p bond distances,[15,16,68−70] (ii) stabilization of the d_π orbitals due to the less effective overlap between the iron (d_π) and porphyrin ($3e_g$) orbitals,[29] and (iii) destabilization of the d_{xy} orbital due to the iron(d_{xy})−porphyrin(a_{2u}) interaction.[48,49] Consequently, the energy levels of the d_π and d_{xy} orbitals are reversed when going from planar $[Fe(TPP)(DMAP)_2]^+$ to ruffled $[Fe(T^iPrP)(DMAP)_2]^+$ complexes as shown in Scheme 4. In this situation, even if the axial DMAP ligand is replaced by a much weaker Py or 4-CNPy, the energy gap between the d_π and the d_{z^2} orbital is still large enough to maintain the low-spin state. Since the 4-CNPy ligand has low-lying p_π^* orbitals, it stabilizes not only the d_{z^2} orbital by its weak σ-donating ability but also the d_π orbitals by its strong π-accepting ability. Therefore, the ruffled $[Fe(T^iPrP)(4\text{-}CNPy)_2]^+$ maintains the $S = {}^1/_2$ state with $(d_{xz}, d_{yz})^4(d_{xy})^1$ electron configuration over a wide range of temperatures, while the saddled $[Fe(ORTPP)(4\text{-}CNPy)_2]^+$ exhibits the spin transition from $S = {}^3/_2$ to $S = {}^1/_2$ at lower temperature. As already mentioned, the replacement of 4-CNPy by a much weaker THF ligand could stabilize the d_{z^2} and d_{xy} orbitals and destabilize the d_π orbital. As a result, four d orbitals of $[Fe(T^iPrP)(THF)_2]^+$ are located very close in the energy diagram as shown in Scheme 4, resulting in the formation of a pure intermediate-spin complex over a wide range of temperatures: ^{1}H NMR, δ(Py−H) = −52.1 ppm (233 K); EPR, $g_\perp = 3.99$ and $g_\perp = 1.97$ (4.2 K); SQUID, $\mu_{eff} = 3.90 \pm 0.10\ \mu_B$ (50−300 K); Mössbauer, IS (76 K) = 0.34 mm s^{-1}, and QS (76 K) = 3.71 mm s^{-1}; X-ray, av Fe−N_p = 1.967(12) Å.[12,15]

Conclusions

Combined analyses using ^{1}H NMR, ^{13}C NMR, and EPR spectroscopy and magnetic measurements revealed that the saddle-shaped $[Fe(OMTPP)L_2]^+$ and $[Fe(TBTXP)L_2]^+$ (L = DMAP, Py, 4-CNPy, THF) complexes exhibit different spin states in solution which depend on the axial ligands. While the DMAP and THF complexes maintain the $S = {}^1/_2$ and $S = {}^3/_2$ spin states, respectively, over a wide temperature range, the Py and 4-CNPy complexes exhibited a spin transition from $S = {}^3/_2$ to $S = {}^1/_2$ as the temperature decreased. Therefore, the magnetic behavior of these complexes is very similar to that of the corresponding $[Fe(OETPP)L_2]^+$ recently reported. The low-spin $[Fe(OMTPP)L_2]^+$ and $[Fe(TBTXP)L_2]^+$ (L = Py and 4-CNPy) complexes formed at low temperature exhibited, however, a different electron configuration from that of the corresponding $[Fe(OETPP)L_2]^+$; the former adopt the $(d_{xz}, d_{yz})^4(d_{xy})^1$ while the latter exhibit the $(d_{xy})^2(d_{xz}, d_{yz})^3$ electron configuration. These results have been explained in terms of the difference in rigidity of the porphyrin cores: while the OMTPP and TBTXP complexes can ruffle the porphyrin core with relatively small energy and change the electronic ground state from $(d_{xy})^2(d_{xz}, d_{yz})^3$ to $(d_{xz}, d_{yz})^4(d_{xy})^1$, the OETPP complexes maintain the saddled structure due to the core rigidity.

Acknowledgment. This work was supported by the Grant in Aid (14540521) for Scientific Research to M.N. from Ministry of Education, Culture, Sports, Science and Technology, Japan. M.N. also thanks the Futaba Memorial Foundation for financial support. T. I. is grateful to the JSPS Research Fellowship for young scientists. Thanks are due to the Research Center for Molecular Materials, the Institute for Molecular Science (IMS), and Louisiana State University.

Supporting Information Available: Curie plots of the *ortho* and *para* protons in $[Fe(OMTPP)L_2]^+$. This material is available free of charge via the Internet at http://pubs.acs.org.

IC0300969

(67) Goff, H. M. *J. Am. Chem. Soc*. **1981**, *103*, 3714−3722.
(68) Scheidt, W. R.; Kirner, J. L.; Hoard, J. L.; Reed, C. A. *J. Am. Chem. Soc*. **1987**, *109*, 1963−1968.
(69) Munro, O. Q.; Marques, H. M.; Debrunner, P. G.; Mohnrao, K.; Scheidt, W. R. *J. Am. Chem. Soc*. **1995**, *117*, 935−954.
(70) Ohgo, Y.; Ikeue, T.; Saitoh, T.; Nakamura, M. *Chem. Lett*. **2002**, 432−433.